An Implementation of Ensemble and Extended Filtering Methods to Estimate Drag and Yaw Coefficients on Amphibious Aircraft Trajectories

Teguh Herlambang
Department of Information System, Universitas Nahdlatul Ulama Surabaya, Indonesia | Center for Data and Business Intelligence, Universitas Nahdlatul Ulama Surabaya, Indonesia
teguh@unusa.ac.id

Zuraini Othman
Department of Diploma Studies, Fakulti Teknologi Maklumat dan Informasi, Universiti Teknikal Malaysia Melaka, Malaysia
zuraini@utem.edu.my

Rachman Sinatriya Marjianto
Department of Engineering, Faculty of Vocational, Universitas Airlangga, Surabaya, Indonesia
rachmansinatriya@vokasi.unair.ac.id (corresponding author)

Sharifah Sakinah Syed Ahmad
Department of Intelligent Computing and Analytics, Faculty of Artificial Intelligence and Cyber Security, Universiti Teknikal Malaysia Melaka, Malaysia
sakinah@utem.edu.my

Sayuti Syamsuar
Research Center for Transportation Technology, National Research and Innovation Agency, KST BJ Habibie, South Tangerang, Banten, Indonesia
sayu001@brin.go.id

Sulistiya
Research Center for Transportation Technology, National Research and Innovation Agency, KST BJ Habibie, South Tangerang, Banten, Indonesia
suli014@brin.go.id

Mohd Sanusi Azmi
Department of Software Engineering, Fakulti Teknologi Maklumat dan Informasi, Universiti Teknikal Malaysia Melaka, Malaysia
sanusi@utem.edu.my

Beny Halfina
Research Center for Transportation Technology, National Research and Innovation Agency, KST BJ Habibie, South Tangerang, Banten, Indonesia
beny002@brin.go.id

Ilham Akbar Adi Satriya
Research Center for Aeronautics Technology, National Research and Innovation Agency, KST BJ Habibie, South Tangerang, Banten, Indonesia
ilham011@brin.go.id

Received: 16 August 2025 | Revised: 30 September 2025 and 6 November 2025 | Accepted: 22 November 2025

 DOI: https://doi.org/10.48084/etasr.14116

ABSTRACT

Indonesia is a strategically significant archipelagic nation with approximately two-thirds of its territory consisting of water. This geographical condition gives Indonesia greater potential than other countries. Amphibious aircraft serve as an alternative solution for the mobility and utility of residents living in remote areas surrounded by water, ensuring that these individuals can benefit from fair and equitable government services and their continuous development is necessary to maximize their functionality. This development encompasses various aspects, including the accuracy of flight trajectory estimation. Several machine learning methods have been developed for estimating the flight trajectory of amphibious aircraft. The present study implements and compares two filtering methods, namely the Ensemble Kalman Filter (EnKF) and the Extended Kalman Filter (EKF). The simulation result indicates that the EnKF method achieved a Root Mean Square Error (RMSE) value of 0.0214 for estimating the drag coefficient (CD) and the EKF method attained 0.0186. Furthermore, the EnKF method recorded an RMSE value of 0.0015 for estimating the yaw coefficient (CY), while the EKF method achieved 0.0012.

Keywords-amphibious aircraft; estimation; ensemble Kalman filter; extended Kalman filter; trajectory

I. INTRODUCTION

As the largest archipelagic nation in the world, Indonesia comprises 16,506 islands, each exhibiting distinct typological and geographical characteristics. This diversity contributes to the rich cultural heritage, traditions, and customs of the Indonesian people [1]. Given this situation, there is a pressing need for a transportation mode that is adaptable to these conditions to facilitate the movement of people and goods. A solution for this transportation challenge is the development of amphibious aircraft, specifically a plan to develop the versatile amphibious version [2].

The presence of amphibious aircraft can play a significant role in this context, despite the fact that its technical development has been stagnant for nearly half a century [3]. Amphibious aircraft fundamentally possess high mobility capabilities. These aircraft are designed to take off and land on water. To facilitate take-off and landing on aquatic surfaces, amphibious aircraft require floats as a substitute for the wheels typically used for land operations [4]. The design of amphibious aircraft encompasses not only its structural construction but also the guidance and navigation systems. Advanced, precise, and accurate guidance and navigation systems facilitate the pilot's operation of the aircraft. Consequently, researchers are engaged in ongoing development and testing to assess trajectory accuracy, aiming to ensure that the safety factors associated with amphibious aircraft are adequately addressed. The present study focuses on comparing the performance of trajectory estimation for the drag coefficient (CD) and yaw coefficient (CY) using the EnKF and EKF methods. Specifically, this study tested EnKF's performance in estimating trajectories based on the size of the ensemble and compared it with EKF's robustness.

Authors in [5] employed EnKF to estimate the water momentum and propeller velocity. EKF, which uses first-order linearization of a nonlinear system through Taylor's expansion, is a modification of the KF algorithm and is frequently applied for nonlinear system models [6]. However, it has a high computational cost. This method has been previously used to estimate the trajectory of Autonomous Surface Vehicles (ASV) [7] and aircraft [8], along with KF, which is utilized to estimate the trajectory of vehicles [9].

II. AMPHIBIOUS AIRCRAFT MODEL

The forces acting on unmanned seaplanes can be categorized into seaplane weight, hydrodynamic force, aerodynamic force, and engine thrust, as shown in Figures 1 and 2. The Earth's coordinate system is denoted as X_e, Y_e, Z_e. The subsequent system of coordinates includes the aircraft's body axis system X_b, Y_b, Z_b, and steady-translation coordinate system X_s, Y_s, Z_s. The motion of the amphibious aircraft is estimated by:

$$m\dot{V} = T\cos(\alpha + \alpha_t) - D_a - N_w \sin\alpha - D_f \cos\alpha + G_{xa} \quad (1)$$

$$mV\dot{\alpha} = mVq - T\sin(\alpha + \alpha_t) - L_a - N_w \cos\alpha + D_f \sin\alpha + G_{za} \quad (2)$$

$$I_y\dot{q} = M_a + M_w + M_T \quad (3)$$

$$\dot{\theta} = q \quad (4)$$

$$\dot{x}_g = u\cos\theta + w\sin\theta \quad (5)$$

$$\dot{z}_g = -u\sin\theta + w\cos\theta \quad (6)$$

In the amphibious aircraft motion estimation model, a discrete model is implemented in the EnKF and EKF algorithms, where this study uses the finite difference method (forward difference method):

If $u = u(x)$, expanded according to the Taylor series, then:

$$u(x+h) = u(x) + h\frac{\partial}{\partial x}u(x) + \frac{h^2}{2!}\frac{\partial^2}{\partial x^2}u(x) + \ldots \quad (7)$$

$$u(x-h) = u(x) - h\frac{\partial}{\partial x}u(x) + \frac{h^2}{2!}\frac{\partial^2}{\partial x^2}u(x) - \ldots \quad (8)$$

Several numerical schemes of the finite difference method are used, namely the forward finite difference from (7), which leads to:

$$u(x+h) - u(x) = h\frac{\partial}{\partial x}u(x) + V(h) \quad (9)$$

$$\frac{u(x+h)-u(x)}{h} \approx \frac{\partial u}{\partial x} \quad (10)$$

Equation (8) is called a forward finite difference equation. If finite difference notation is used with $u = (x = ih)$, (8) becomes:

$$\frac{\partial u}{\partial x} = \frac{u_{i+1}-u_i}{\Delta x} \quad (11)$$

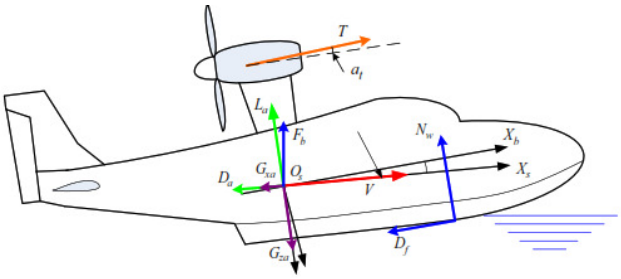

Fig. 1. Forces acting on the amphibious aircraft.

TABLE I. DESCRIPTION OF TERMS USED FOR THE AMPHIBIOUS AIRCRAFT MODEL

Symbol	Description	Symbol	Description
α	Angle of attack	m	Weight of the amphibious aircraft
Θ	Angle of pitch	D_a	Aerodynamic drag style
V	Velocity	G_{xa}	Gravitational force along X_s
α_t	Angle between the machine force and the surface *Xb*	G_{za}	Gravity along Z_s
M_a	Total pitching moment from air	X_g	Aircraft's position along the route X_e
M_w	Total pitching moment from water	Z_g	Aircraft's position along the route Z_e
M_T	Total pitching moment from the machine	u	Component of the aircraft's speed throughout X_b
T	Style of engine propulsion	w	Components of an aircraft's speed throughout Z_b
N_w	Water pressure directed normally at the lower section of the aircraft	q	Angular pitch rate
D_f	Friction of water along the underside of the aircraft	I_y	Moment of inertia of an amphibious aircraft Y_b
L_a	Aerodynamic lift	$\dot{\Theta}$	Change in tilt angle
$\dot{V}$	Change in speed	$\dot{\alpha}$	Change in attack angle

Fig. 2. Aerodynamic model of seaplane during wind tunnel test.

III. DATA AND MODELLING

The dataset utilized is derived from a wind tunnel test. The experimental data were collected during runs 21-32 and consist of 260 rows and 6 columns, as presented in Table II. Figures 3 and 4 depict the plots of the actual coefficient values.

TABLE II. DATASET

Run	Alfa	Beta	CL	CD	CY
21	10.3566	0	-0.5113	0.2527	-0.0055
21	-9.3566	0	-0.4751	0.2262	-0.0052
21	-8.27	0	-0.3783	0.1921	-0.0079
21	-7.1233	0	-0.1754	0.155	-0.008
21	-6.0	0	0.0058	0.13403	-0.0068
21	-4.9	0	0.1426	0.1259	-0.0042
21	-3.82	0	0.2792	0.1223	-0.0041
21	-2.73	0	0.4112	0.1204	-0.0027
21	-1.63	0	0.5425	0.1195	-0.0021
21	-0.5333	0	0.6708	0.1205	-0.0016
32	16.2683	0	2.1692	0.4242	-0.0154

The employed filtering methods are EnKF and EKF. EnKF is an effective advancement of the Kalman filter technique, utilized for solving non-linear problems [10]. This method was proposed in [11]. The general form of the nonlinear dynamic system in the EnKF is [12]:

$$x_{k+1} = f(k, x_k) + w_k \quad (12)$$

Utilizing linear measurements, $z_k \in \Re^p$ leads to:

$$z_k = Hx_k + v_k \quad (13)$$

$$x_0 \sim N(\overline{x_0}, P_{x_0}); w_k \sim N(0, Q_k); v_k \sim N(0, R_k) \quad (14)$$

The estimation process in the EnKF begins with the generation of a set of ensembles characterized by a mean of zero and a covariance of one. The ensembles are generated randomly and follow a normal distribution:

$$X_{0,i} = [x_{0,1} \quad x_{0,2} \quad x_{0,3} \quad \ldots\ldots \quad x_{0,Ne}] \quad (15)$$

The prediction and correction phase is similar to the Kalman Filter method; however, before entering the prediction stage, the ensemble mean is determined by:

$$\hat{x}_k^* = \frac{1}{N_e}\sum_{i=1}^{N} x_{k,i} \quad (16)$$

The error covariance can be determined by:

$$P_k = \frac{1}{N_e - 1} \sum_{i=1}^{N} (\hat{x}_{k,i}^- - \hat{x}_k^-)(\hat{x}_{k,i}^- - \hat{x}_k^-)^T \quad (17)$$

Equation (11) is utilized during the prediction and correction phases to calculate the estimates for each component $\hat{x}_k^-$ and $\hat{x}_k$. Equation (12) is exclusively utilized for covariance during the prediction phase. In the EnKF, the system noise w_k during the prediction phase and the measurement noise v_k during the correction phase are generated in the form of an ensemble.

EKF incorporates a linearization step for non-linear systems, utilizing first-order Taylor expansion to perform linearization around the current estimate. The optimality of EKF is demonstrated when the linearization is conducted around the precise value of the state vector. The following outlines the mathematical functions associated with the EKF method [13].

$$M_{k+1} = \left(rM(t) - \frac{r}{K} M^2(t)\right)\Delta t + M_k + w1_k \quad (18)$$

$$N_{k+1} = \left(-\frac{r}{K^2} {N_k}^3 + rN_k\right)\Delta t + N_k + w_{2k} \quad (19)$$

$$z_{1k} = HM_k + v_k \quad (20)$$

$$z_{2k} = HN_k + v_k \quad (21)$$

where w_k and v_k represent white noise, which is uncorrelated and normally distributed with:

$$E\{w_k\} = 0 \quad (22)$$

$$Cov\{w_k, w_k\} = E(w_k, w_k)^T = Q \quad (23)$$

and:

$$E\{v_k\} = 0 \quad (24)$$

$$Cov\{v_k, v_k\} = E(v_k, v_k)^T = R \quad (25)$$

This allows the following:

$$w_k \sim N(0, Q) \quad (26)$$

$$v_k \sim N(0, R) \quad (27)$$

where Q and R represent the variances of noise.

Subsequently, the initial initialization is carried out at $t = 0$

$$P_0 = \begin{bmatrix} PM_0 & 0 \\ 0 & PN_0 \end{bmatrix};\ \widehat{M_0} = \overline{M_0};\ \widehat{N_0} = \overline{N_0} \quad (28)$$

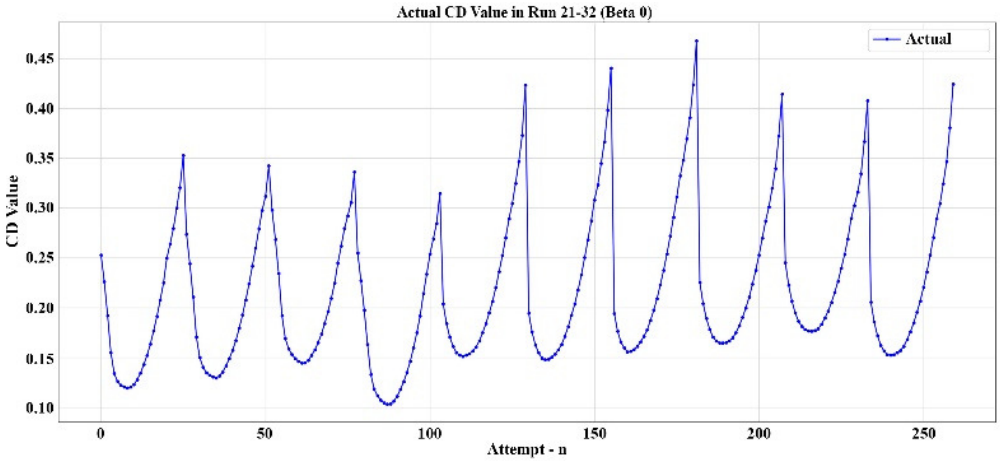

Fig. 3. Plot of actual CD.

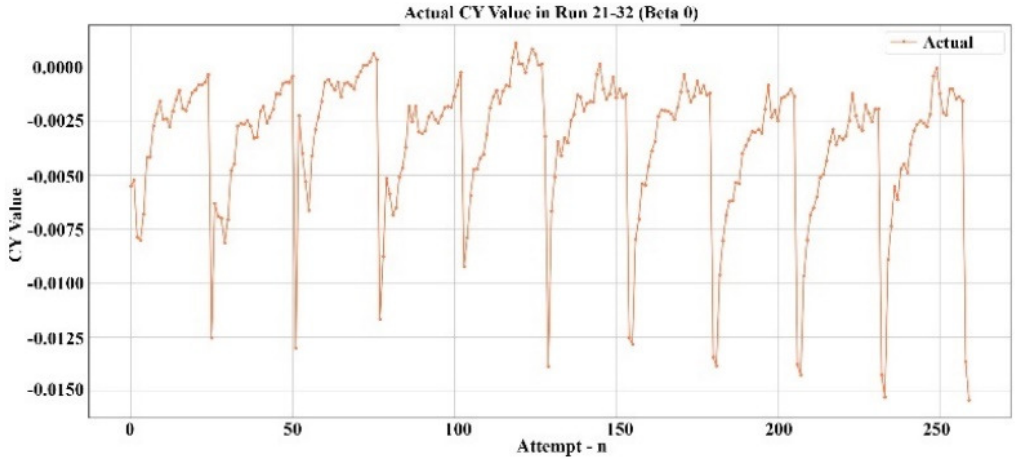

Fig. 4. Plot of actual CY.

1) Measurement System Model

2) Prediction Stage

$$\widehat{M}_{\overline{k+1}} = \left(rN(t) - \frac{r}{K}N^2(t)\right)\Delta t + M_k \quad (29)$$

$$\widehat{N}_{\overline{k+1}} = \left(-\frac{r}{K^2}Nk^3 + rN_k\right)\Delta t + N_k \quad (30)$$

3) Calculation of Error Covariance

$$P_{\overline{k+1}} = AP_kA^T + Q \quad (31)$$

4) Correction Stage

Calculating the Kalman Gain to minimize the prediction error covariance:

$$K_{k+1} = P_{\overline{k+1}}H^T(HP_{\overline{k+1}}H^T + R)^{-1} \quad (32)$$

Subsequently, the estimated value at the correction stage is calculated by adding the Kalman Gain matrix multiplied by $(Z_{k+1} - H_{\widehat{X}_{\overline{k+1}}})$ for each model, resulting in:

$$\widehat{M}_{k+1} = \widehat{M}_{\overline{k+1}} + K_{k+1}(z_{1k+1} - H\widehat{M}_{\overline{k+1}}) \quad (33)$$

$$\widehat{N}_{k+1} = \widehat{N}_{\overline{k+1}} + K_{k+1}(z_{2k+1} - H\widehat{N}_{\overline{k+1}}) \quad (34)$$

The covariance value of the error during the correction phase is determined by:

$$P_{k+1} = [I - K_{k+1}H]P_{\overline{k+1}} \quad (35)$$

IV. RESULTS AND DISCUSSION

A. Simulation to Estimate the Drag Coefficient

The results of the CD simulation, conducted using EnKF and EKF are illustrated in Figures 5 and 6. Figure 5 displays the initial simulations of the CD values, conducted using EnKF with 200 ensembles and EKF. For this step, the observation model of the EnKF was configured with a value of 0.9, utilizing an ensemble size of 200, while the *R* value was set to 0.01, consistent with that of the EKF. The estimation obtained from the EnKF method produced an RMSE value of 0.0219, as illustrated by the blue line, which closely aligns with the actual values represented by the red line. In contrast, the estimation from EKF, indicated by the black line, also demonstrates a close approximation to the actual values. The EKF method resulted in an RMSE of 0.0186.

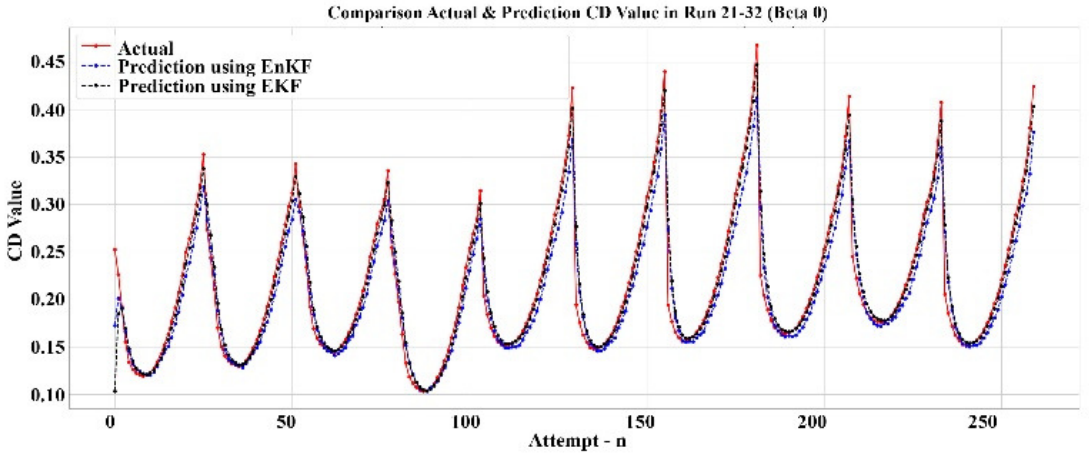

Fig. 5. First simulation plot of estimated CD values using EnKF and EKF.

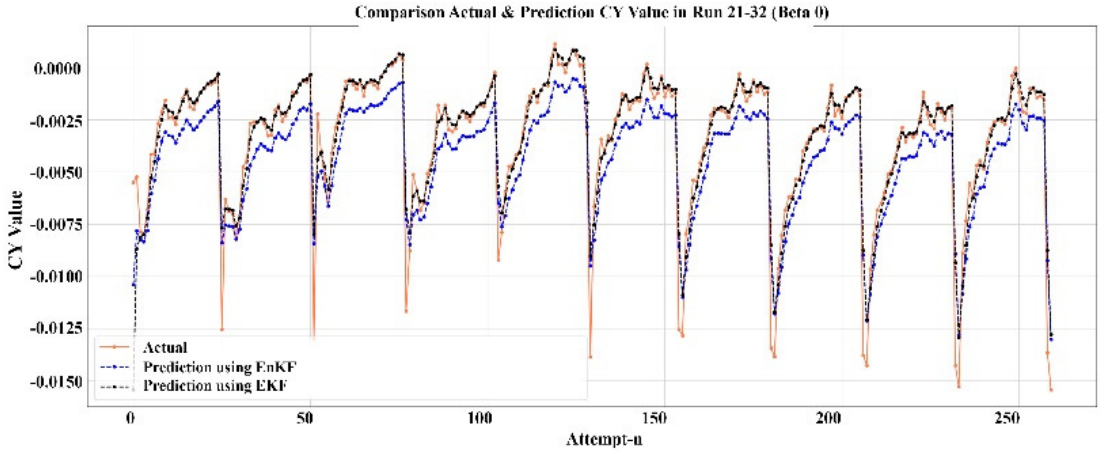

Fig. 6. First simulation plot of estimated CY values using EnKF and EKF.

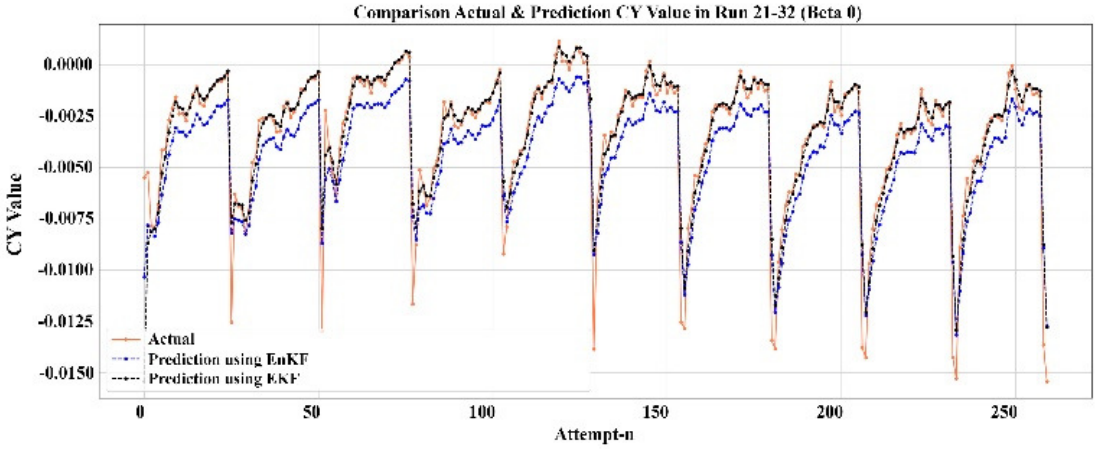

Fig. 7. Second simulation plot of estimated CY values using EnKF and EKF.

Figure 6 illustrates the second simulation of the CD values, conducted using EnKF with 300 ensembles and EKF. For this step, the observation model of the EnKF was configured with a value of 0.9, utilizing an ensemble size of 300, while the *R* value was set to 0.01, consistent with that of the EKF. The estimation obtained from EnKF achieved an RMSE value of 0.0214 represented by the blue line and the estimation from EKF, indicated by the black line, demonstrates a closer approximation to the actual values. EKF achieved an RMSE value of 0.0186.

B. Simulation for the Estimation of Yaw Coefficient

Subsequently, the simulation continued to estimate the CY using EnKF and EKF. Figure 7 illustrates the results of the first CY simulation using EnKF with an ensemble size of 200 and EKF. For this step, the EnKF observation model was set with a value of 0.9, an ensemble size of 200, and an *R* value of 0.01, similar to that of EKF. The estimation of the EnKF obtained an RMSE of 0.00155 and the estimation result of EKF produced an RMSE value of 0.00125. Figure 8 illustrates the results of the second CY simulation, conducted using EnKF with an ensemble size of 300 and EKF. For this step, the observation model for the EnKF was configured with a value of 0.9, maintaining the ensemble size at 300, and the *R* value was consistent with that of the EKF, set at 0.01. The estimation from the EnKF achieved an RMSE of 0.00154 and the estimation results from EKF obtained an RMSE of 0.00125. It is seen that the RMSE value from EKF remains superior to that of the EnKF, despite a reduction in the RMSE for EnKF. Table III summarizes the EnKF simulation results for the CD estimation, while Table IV shows the simulation results for CY estimation.

TABLE III. COMPARISON RMSE OF COEFFICIENT DRAG ESTIMATION

Method	Simulation	RMSE
EnKF	1	0.0219
	2	0.0214
EKF	1	0.0186
	2	

TABLE IV. COMPARISON RMSE OF COEFFICIENT YAW ESTIMATION

Method	Simulation	RMSE
EnKF	1	0.0015
	2	0.0015
EKF	1	0.0012
	2	

V. CONCLUSION

Based on the results of the simulations conducted, it can be concluded that the Ensemble Kalman Filter (EnKF) and Extended Kalman Filter (EKF) methods successfully estimated the drag (CD) and the yaw coefficient (CY). The best CD estimation using EnKF was observed in the second simulation, which achieved a Root Mean Square Error (RMSE) of 0.0214, with an ensemble size of 300, an observation model of 0.9, and an *R* value of 0.01, while EKF achieved a better RMSE value of 0.0186. Furthermore, the simulations for estimating CY using EnKF showed the same RMSE values (0.0015) in all simulations. In contrast, the optimal results for estimating CY using EKF were noted with an *R* value of 0.01 and an RMSE of 0.0012.

The RMSE value obtained from the simulation, which was mainly conducted on CD, demonstrates that the error does not affect the stability and control of the amphibious aircraft.

Overall, the results obtained from EnKF and EKF are still considered satisfactory and consistent. Thus, these methods can be proposed for use in future research.

ACKNOWLEDGEMENT

This research was supported by the RIIM LPDP Grant and BRIN 2022-2024 with an agreement letter number B-802/II.7.5/FR/6/2022 and B-9106/III.3/KS.00.00/9/2022. The authors also thank LPPM Universitas Nahdlatul Ulama for research collaboration and extend their deepest gratitude to the Universiti Teknikal Malaysia Melaka (UTeM) and MRL Engineering Sdn Bhd for the financial support provided through the University-Industry Research Matching Grant

(URMG). This work was supported by GRANT No: INDUSTRI(URMG)/MRL/FTMK/2024/I00094.

REFERENCES

[1] A. J. Astari, S. A. Aliyan, A. S. Bratanegara, A. B. Muslim, V. I. Nurawaliyah, and A. A. A. Mohamed, "Understanding the Scope of Regional Geography: A Perspective from Indonesia's Geographic Region," *E3S Web of Conferences*, vol. 600, 2024, Art. no. 02018, https://doi.org/10.1051/e3sconf/202460002018.

[2] E. C. K. Putra *et al.*, "Technological Developments of Amphibious Aircraft Designs: Research Milestone and Current Achievement," *Curved and Layered Structures*, vol. 12, no. 1, May 2025, Art. no. 20250026, https://doi.org/10.1515/cls-2025-0026.

[3] D. Arianto, Iskendar, W. P. Humang, E. Marpaung, J. Malisan, and F. S. Puriningsih, "Operational Feasibility of Water-Based Development for Amphibious Aircraft to Support Sustainable Tourism in Indonesia's Small Islands," in *Proceedings of the 10th International Conference on Sustainable Energy Engineering And Application 2022*, Tangerang Selatan, Indonesia, 2024, Art. no. 020125, https://doi.org/10.1063/5.0206508.

[4] J. Lyu, R. Yang, and L. Huang, "Structure Dynamic Response of Amphibious Aircraft Induced by Water-Taxiing," *International Journal of Aerospace Engineering*, vol. 2021, pp. 1–10, Nov. 2021, https://doi.org/10.1155/2021/6104407.

[5] B. A. Iza, Q. A. Fiddina, H. N. Fadhilah, D. K. Arif, and Mardlijah, "Automatic Guided Vehicle (AGV) tracking model estimation with Ensemble Kalman Filter," in *7th International Conference on Mathematics: Pure, Applied And Computation: Mathematics Of Quantum Computing*, Surabaya, Indonesia, 2022, Art. no. 030019, https://doi.org/10.1063/5.0118817.

[6] T. Omeragic and J. Velagic, "Tracking of Moving Objects Based on Extended Kalman Filter," in *2020 International Symposium ELMAR*, Zadar, Croatia, Sept. 2020, pp. 137–140, https://doi.org/10.1109/ELMAR49956.2020.9219021.

[7] H. H. Al Malki, A. I. Moustafa, and M. H. Sinky, "An Improving Position Method Using Extended Kalman Filter," *Procedia Computer Science*, vol. 182, pp. 28–37, 2021, https://doi.org/10.1016/j.procs.2021.02.005.

[8] W. Farag, "Kalman-filter-Based Sensor Fusion Applied to Road-objects Detection and Tracking for Autonomous Vehicles," *Proceedings of the Institution of Mechanical Engineers, Part I: Journal of Systems and Control Engineering*, vol. 235, no. 7, pp. 1125–1138, Aug. 2021, https://doi.org/10.1177/0959651820975523.

[9] P. Chen, L. Wei, F. Meng, and N. Zheng, "Vehicle Trajectory Reconstruction for Signalized Intersections: A Hybrid Approach Integrating Kalman Filtering and Variational Theory," *Transportmetrica B: Transport Dynamics*, vol. 9, no. 1, pp. 22–41, Jan. 2021, https://doi.org/10.1080/21680566.2020.1781707.

[10] Z. Zhang, K. Fu, X. Sun, and W. Ren, "Multiple Target Tracking Based on Multiple Hypotheses Tracking and Modified Ensemble Kalman Filter in Multi-Sensor Fusion," *Sensors*, vol. 19, no. 14, July 2019, Art. no. 3118, https://doi.org/10.3390/s19143118.

[11] S. E. Prakosa *et al.*, "Comparison of Ensemble Kalman Filter, Unscented Kalman Filter, and Fractional Kalman Filter for estimating the concentration of CO2 and NO2," *Journal of Physics: Conference Series*, vol. 1821, no. 1, Mar. 2021, Art. no. 012052, https://doi.org/10.1088/1742-6596/1821/1/012052.

[12] T. Herlambang, F. A. Susanto, D. Adzkiya, A. Suryowinoto, and K. Oktafianto, "Design of Navigation and Guidance Control System of Mobile Robot with Position Estimation Using Ensemble Kalman Filter (EnKF) and Square Root Ensemble Kalman Filter (SR-EnKF)," *Nonlinear Dynamics and Systems Theory*, vol. 22, no. 4, pp. 390–399, Sept. 2022.

[13] D. Zhan, H. Zheng, and W. Xu, "Tracking Control of Autonomous Underwater Vehicles with Acoustic Localization and Extended Kalman Filter," *Applied Sciences*, vol. 11, no. 17, Aug. 2021, Art. no. 8038, https://doi.org/10.3390/app11178038.